Virologica Sinica 40 (2025) 333–339

Contents lists available at ScienceDirect

Virologica Sinica

journal homepage: www.keaipublishing.com/en/journals/virologica-sinica
www.virosin.org

Research Article

Differential susceptibility of immunodeficient mice to MPXV infection and the impact of various inoculation routes

Xiaohan Wang [a,b,1], Shaowen Shi [b,c,1], Xiaoxuan Nie [b,c,1], Yongyang Sun [b,d], Jinglei Hu [b], Manlin He [b,c], Wenhao Ren [b,d], Yuxing Wang [b,d], Zhendong Guo [b], Gonghe Li [a], Changbo Ou [a,*], Xiao Li [b,*], Zongzheng Zhao [b,*]

[a] Guangxi University, Nanning, 530004, China
[b] Changchun Veterinary Research Institute, Chinese Academy of Agriculture Sciences, Changchun, 130122, China
[c] Hebei Agricultural University, Baoding, 071000, China
[d] Jilin Agricultural University, Changchun, 130118, China

ARTICLE INFO

Keywords:
Monkeypox virus (MPXV)
Mouse
Susceptibility
Infection routes
Pathogenicity

ABSTRACT

Monkeypox virus (MPXV), a member of the *Orthopoxvirus* genus, caused a large-scale global outbreak in 2022. Developing mouse models for MPXV infection is crucial for advancing research on vaccines and therapeutic interventions. To address this, we conducted a comparative study on the susceptibility of six mouse strains—severe combined immune-deficiency (SCID), nude, genetically diabetic (db/db) and obese (ob/ob), C57BL/6J, and BALB/c—to MPXV infection. Mouse strains were infected with MPXV via intranasal inoculation, and body weight changes and mortality were monitored post-infection. Additionally, the tissue distribution of MPXV and the pathological changes in the lung tissues of the infected mice were evaluated. The results demonstrated that SCID and nude mice exhibited significant weight loss following MPXV infection, with 100 % mortality observed in SCID mice, while no mortality occurred in nude mice. In contrast, the other mouse strains showed no significant weight loss or mortality. Notably, the viral load in the lung tissues of SCID and nude mice was the highest among the tested strains. Furthermore, we investigated the impact of different inoculation routes—intranasal (I.N.), intraperitoneal (I.P.), and intravenous (I.V.)—on the pathogenicity of MPXV in mice. The results revealed that the intravenous route induced more pronounced pathogenic effects compared to the intranasal and intraperitoneal routes. In summary, this study provides valuable insights into the development of MPXV-infected mouse models, offering a foundation for further research on MPXV pathogenesis and therapeutic drug development.

INTRODUCTION

Monkeypox virus (MPXV) is a zoonotic viral pathogen that presents with clinical features similar to smallpox but typically manifests with milder symptoms (Bunge et al., 2022; Hennessee et al., 2022). MPXV can be transmitted to humans through direct contact with the blood or bodily fluids of infected individuals, as well as through contact with mucosal surfaces or skin lesions of infected animals. Transmission routes include respiratory droplets, contact with bodily fluids, contaminated environments, and skin lesions of infected individuals (Kumar et al., 2022; Laurenson-Schafer et al., 2023; Zhu et al., 2022), posing a potential threat to global public health. Although MPXV has caused outbreaks in multiple regions in recent years, specific treatments and vaccines targeting the virus remain limited. Therefore, establishing animal models of MPXV infection is essential for advancing our understanding of its pathogenesis and developing novel therapeutics and vaccines.

Although most animals do not naturally acquire MPXV infection, certain species can be utilized as experimental models. These animals are generally categorized into non-human primates, wild North American rodents, wild African rodents, and inbred mice. Most non-human

* Corresponding authors.
E-mail addresses: ouchangbo@gxu.edu.cn (C. Ou), lixiao06@mails.jlu.edu.cn (X. Li), 329517286@qq.com (Z. Zhao).
[1] Xiaohan Wang, Shaowen Shi, and Xiaoxuan Nie contributed equally to this work.

https://doi.org/10.1016/j.virs.2025.04.001
Received 17 January 2025; Accepted 2 April 2025
Available online 7 April 2025

primates, such as the Asian cynomolgus monkey, serve as excellent animal models for simulating human MPXV infection and conducting preclinical testing of treatments or preventive measures. However, due to challenges related to housing conditions, high costs, and ethical concerns, non-human primates are less suitable for large-scale or comprehensive studies. Among rodents, wild North American species (e.g., ground squirrels, prairie dogs, and deer mice) and wild African species (e.g., African dormice, rope squirrels, and Gambian pouched rats) exhibit higher susceptibility to MPXV, making them valuable for modeling natural MPXV infections. Nonetheless, the use of wild animals in experimental research is constrained by difficulties in capture and control of individual variability. In comparison, while inbred mice lack the high susceptibility to MPXV seen in non-human primates and wild rodents, they offer significant advantages such as ease of breeding and commercial availability. Therefore, investigating the susceptibility of different inbred mouse strains to MPXV holds considerable significance.

Previous studies have shown that diabetes can enhance the pathogenicity of SARS-CoV-2 in affected patients (Branche et al., 2024). To examine the impact of diabetes on MPXV susceptibility, we selected db/db and ob/ob mice, well-established models of genetic obesity and metabolic dysfunction. The db/db mice carry mutations in the diabetes (db) gene encoding the leptin receptor (ObR), whereas ob/ob mice are characterized by mutations in the obesity (ob) gene encoding leptin (Coleman, 1978), and both models are widely used in research on obesity and related metabolic disorders (Everard et al., 2011; Geurts et al., 2011; Giesbertz et al., 2015). To investigate whether immune deficiencies

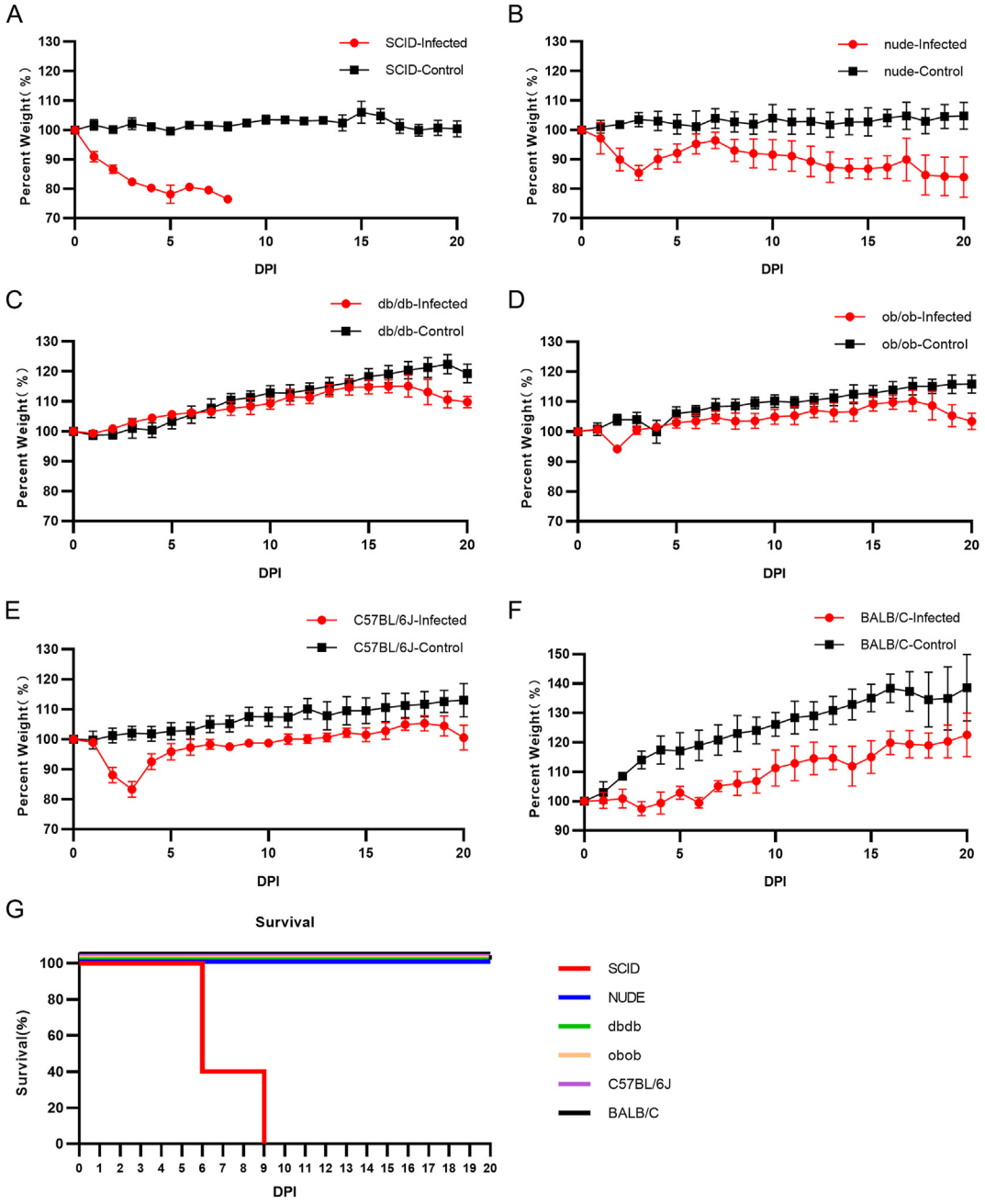

Fig. 1. Body weight changes and mortality rates in different mouse strains following MPXV intranasal infection. Mouse strains were intranasally infected with $10^{5.5}$ $TCID_{50}$ of MPXV, and their body weight changes and mortality were daily monitored. **A–F** The body weight changes of severe combined immune-deficiency (SCID) mice (**A**), nude mice (**B**), db/db mice (**C**), ob/ob mice (**D**), C57BL/6J mice (**E**), and BALB/c mice (**F**), respectively, after infection. (**G**) The mortality rates of the six mouse strains following MPXV intranasal infection. DPI: days post-infection.

affect the susceptibility of mice to MPXV, we included severe combined immune-deficiency (SCID) mice, which have T-cell and B-cell deficiencies, and nude mice, which lack a thymus, as research models. Additionally, C57BL/6J and BALB/C mice, widely used in experimental research due to their accessibility and high reproducibility, were selected as common model organisms. Thus, a total of six mouse strains were chosen for this study.

RESULT

Body weight and mortality in mice after intranasal MPXV infection

To evaluate the susceptibility of SCID, nude, db/db, ob/ob, C57BL/6J, and BALB/C mice to MPXV infection, all six strains were intranasally (I.N.) infected with $10^{5.5}$ $TCID_{50}$ of MPXV, and their body weight changes and mortality were monitored (Fig. 1). The results demonstrated significant weight loss in SCID mice, with body weight decreasing to 75% of baseline by 6 days post-infection (DPI) (Fig. 1A). SCID mice were humanely euthanized when body weight dropped below 75%. Mortality reached 60% by 6 DPI and 100% by 9 DPI (Fig. 1G). SCID mice also exhibited lethargy, ruffled fur, and reduced activity throughout the infection.

In nude mice, body weight decreased to 83.2% by 3 DPI, followed by a gradual recovery to 99.6% by 7 DPI. However, a persistent low-level decline was observed thereafter (ranging from 75.78% to 93.72%; Fig. 1B). In contrast, db/db and ob/ob mice did not show significant weight loss post-infection. While ob/ob mice experienced a slight decline (92.87%) at 2 DPI, their body weight subsequently recovered and paralleled the weight gain of control mice (Fig. 1C and D). Similarly, C57BL/6J mice exhibited a transient weight loss during the first 3 DPI, followed by a gradual recovery and steady weight gain consistent with the control group. BALB/C mice displayed a weight gain trajectory identical to the control group throughout the infection period (Fig. 1E and F).

Aside from SCID mice, none of the other five strains displayed overt clinical symptoms during the study. SCID and nude mice exhibit significant weight loss following MPXV infection, with SCID mice experiencing 100% mortality and nude mice showing no deaths. In contrast, db/db, ob/ob, C57BL/6J, and BALB/C mice did not exhibit significant weight loss or mortality during the infection period.

MPXV viral load in lung tissue of different mice following I.N. inoculation

To assess the replication of MPXV in mouse tissues, $10^{5.5}$ $TCID_{50}$ of MPXV was inoculated via I.N. administration into the six mouse strains. At 6, 12, and 18 DPI, lung tissues were harvested, homogenized, and the viral load was quantified (Fig. 2). At 6, 12, and 18 DPI, the viral loads in the lungs of SCID mice were $10^{5.56\pm0.05}$, $10^{5.80\pm0.09}$, and $10^{5.90\pm0.03}$ copies/mL, respectively. The viral loads in nude mice were $10^{4.84\pm0.02}$, $10^{5.98\pm0.07}$, and $10^{5.74\pm0.60}$ copies/mL, respectively. No MPXV was detected in the lungs of db/db, ob/ob, C57BL/6J, and BALB/C mice. These results indicate that MPXV undergoes replication in the lungs of SCID and nude mice following I.N. infection.

MPXV viral load in different tissues of SCID and nude mice following I.N. inoculation

To investigate the replication of MPXV in various tissues of SCID and nude mice, the viral load of MPXV was measured in seven tissues (liver, spleen, heart, kidney, brain, rectum, and testes) of both SCID and nude mice at 12 DPI (Fig. 3). MPXV was detected in all seven tissues of both SCID and nude mice, with no significant differences in viral load between the tissues. However, the viral load in the tissues of nude mice was consistently higher than that in SCID mice. At 12 DPI, the MPXV viral load in SCID mouse tissues was as follows: liver: $10^{2.40\pm0.04}$, spleen: $10^{3.08\pm0.14}$, heart: $10^{2.57\pm0.12}$, kidney: $10^{2.30\pm0.12}$, brain: $10^{2.48\pm0.08}$, rectum: $10^{2.12\pm0.05}$, testes: $10^{2.19\pm0.08}$. In the tissues of nude mice, the MPXV viral load was: liver: $10^{3.70\pm0.10}$, spleen: $10^{3.56\pm0.04}$, heart: $10^{3.68\pm0.08}$, kidney: $10^{3.40\pm0.16}$, brain: $10^{3.42\pm0.02}$, rectum: $10^{3.16\pm0.30}$, testes: $10^{3.02\pm0.19}$ (Units: copies/mL).

Histopathological examination of lung tissues in SCID and nude mice following I.N. MPXV infection

To assess the histopathological changes in lung tissue following I.N. MPXV infection in SCID and nude mice, we performed histological examinations (Fig. 4). At 6 DPI, the alveolar number in the lung tissue of SCID mice gradually increased, with bronchial structures (indicated by black arrows) showing a small amount of cell debris in the lumen (Fig. 4B). At 12 DPI, moderate structural abnormalities began to appear in the lung tissue, with regions showing substantial alveolar collapse and epithelial cell proliferation, along with mild infiltration of inflammatory cells (indicated by red arrows) (Fig. 4C). By 18 DPI, the structural damage in SCID mice's lung tissue showed slight improvement with no significant inflammatory cell infiltration (Fig. 4D). In nude mice, lung tissue changes progressed with time, becoming moderately abnormal by 18 DPI (Fig. 4E–H), with thickening of the alveolar walls (indicated by blue arrows) (Fig. 4F and G). There was an increase in epithelial cells and inflammatory cells (indicated by red arrows) (Fig. 4G and H), and signs of cell necrosis and nuclear fragmentation were observed (indicated by

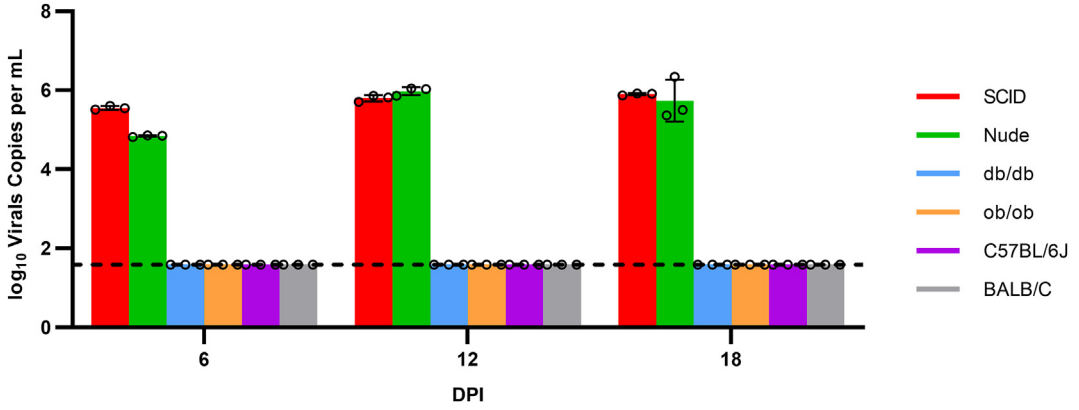

Fig. 2. MPXV viral loads in the lung tissues of different mouse strains following MPXV intranasal infection. Mouse strains were intranasally infected with $10^{5.5}$ $TCID_{50}$ of MPXV. The viral loads in the lung tissues at day 6, 12, and 18 post-infection were determined by qRT-PCR. Each mouse strain group consisted of three individuals. Data are presented as mean ± SEM. DPI: days post-infection.

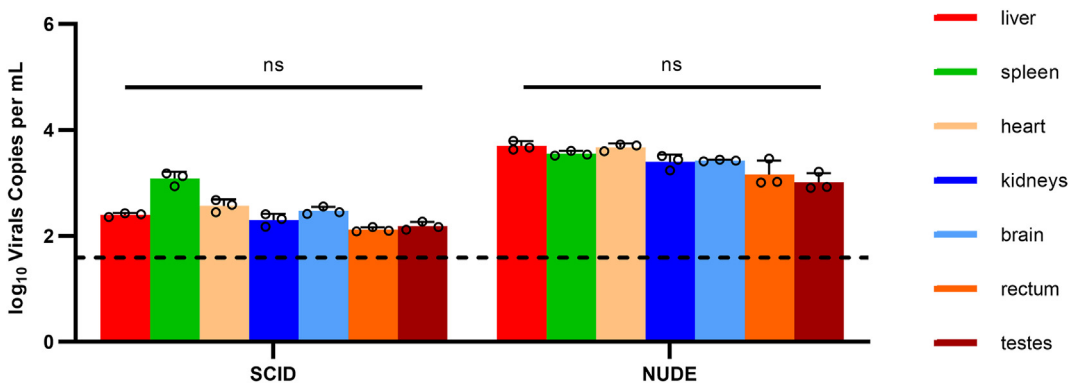

Fig. 3. MPXV viral loads in different tissues of severe combined immune-deficiency mice (SCID) and nude mice at 12 days post-infection. Mouse strains were intranasally infected with $10^{5.5}$ $TCID_{50}$ of MPXV. The viral loads in tissues at day 12 post-infection were determined by qRT-PCR. Each mouse strain group consisted of three individuals. Data are presented as mean ± SEM.

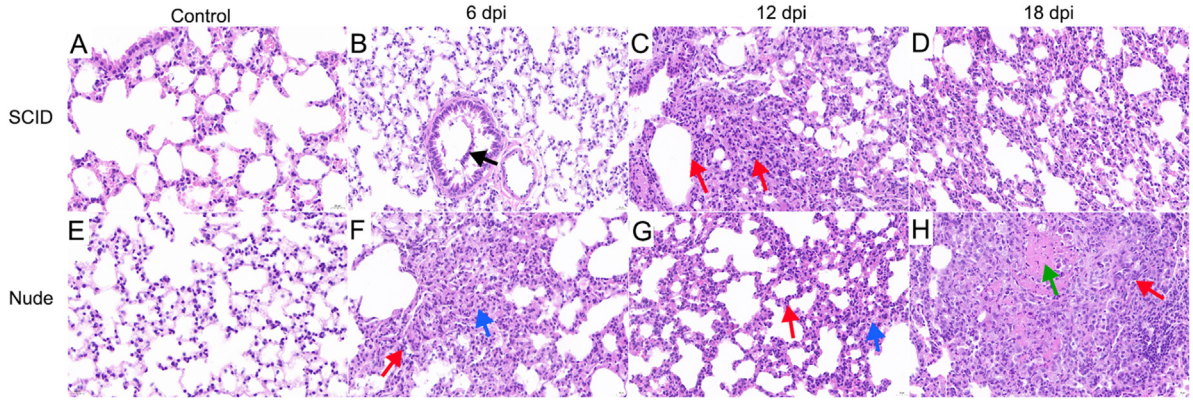

Fig. 4. Histopathological changes in the lung tissues of severe combined immune-deficiency (SCID) mice and nude mice. SCID mice and nude mice were intranasally infected with $10^{5.5}$ $TCID_{50}$ of MPXV. The lung tissues were collected at day 6, 12, and 18 post-infection for histopathological analysis. **A–D** Lung tissue from SCID mice exhibited progressive structural abnormalities over time, transitioning from normal to moderately abnormal, with epithelial cell proliferation (indicated by black arrows) and mild inflammatory cell infiltration observed (indicated by red arrows). At 18 DPI, these pathological changes showed signs of gradual resolution. **E–H** Lung tissue from nude mice demonstrated a time-dependent progression from normal to moderate abnormalities, characterized by thickened alveolar walls (indicated by blue arrows), extensive inflammatory cell infiltration, and localized necrosis of some cells (indicated by green arrows). Hematoxylin and eosin staining, 40× magnification. dpi: days post-infection.

green arrows) (Fig. 4H). These results suggest that I.N. MPXV infection causes lung damage in both SCID and nude mice.

Body weight changes and mortality in SCID and nude mice following MPXV infection via different routes

To assess the pathogenic differences resulting from different infection routes, SCID and nude mice were intranasally (I.N.), intraperitoneally (I.P.), or intravenously (I.V.) inoculated with $10^{4.5}$ $TCID_{50}$ MPXV (100 μL), and their body weight changes were monitored for three weeks (Fig. 5). The reason for using a lower viral dose in this study is that SCID mice exhibited significant infection responses and high mortality at $10^{5.5}$ $TCID_{50}$. To better evaluate the impact of different inoculation routes on infection outcomes, we reduced the viral dose in this study. Notably, the SCID mice infected via the I.V. route exhibited more significant body weight loss than those infected via the I.N. and I.P. routes (Fig. 5A). As in previous experiments, SCID mice were euthanized once their body weight decreased to 75% of the initial weight. The I.V.-infected SCID mice experienced a significant weight loss, with body weight dropping below 75% by 11 DPI, resulting in a mortality rate of 20% at 11 DPI, 80% at 12 DPI, and 100% at 15 DPI. These mice also displayed clinical signs, including poor appetite, rough fur, and reduced activity. In contrast, SCID mice infected via the I.N. and I.P. routes did not exhibit significant weight loss, clinical symptoms, or mortality. For nude mice, no significant weight loss was observed with I.N. and I.P. infection, while the I.V. infection led to a slight weight decline, which was less severe than in the I.V.-infected SCID mice, and no mortality was recorded (Fig. 5B). Overall, intravenous infection with MPXV caused more pronounced body weight loss in mice than intranasal and intraperitoneal infections.

MPXV viral load in tissues of SCID and nude mice following infection via different routes

To determine the distribution of MPXV in tissues following different infection routes in SCID mice and nude mice, we assessed the viral load in the lungs, liver, spleen, and whole blood at 9 DPI (Fig. 6). The results revealed that SCID mice infected via the I.V. route exhibited higher viral loads in both lungs and blood, with a significantly higher viral load in the blood compared to SCID mice infected via I.N. Additionally, no significant difference was observed in the viral load between the lungs of I.V.-infected and I.N.-infected SCID mice (Fig. 6A). In nude mice, the viral load in the lungs and blood was higher following I.V. infection compared to the liver and spleen. Notably, the viral load in the blood of I.V.-infected nude mice was significantly higher than that of I.N.-infected mice. However, the viral load in the lungs of I.N.-infected nude mice was significantly higher than that in I.V.-infected mice (Fig. 6B). These results suggest that, in both SCID and nude mice, I.V. infection results in significantly higher viral loads in the blood compared to I.N. infection.

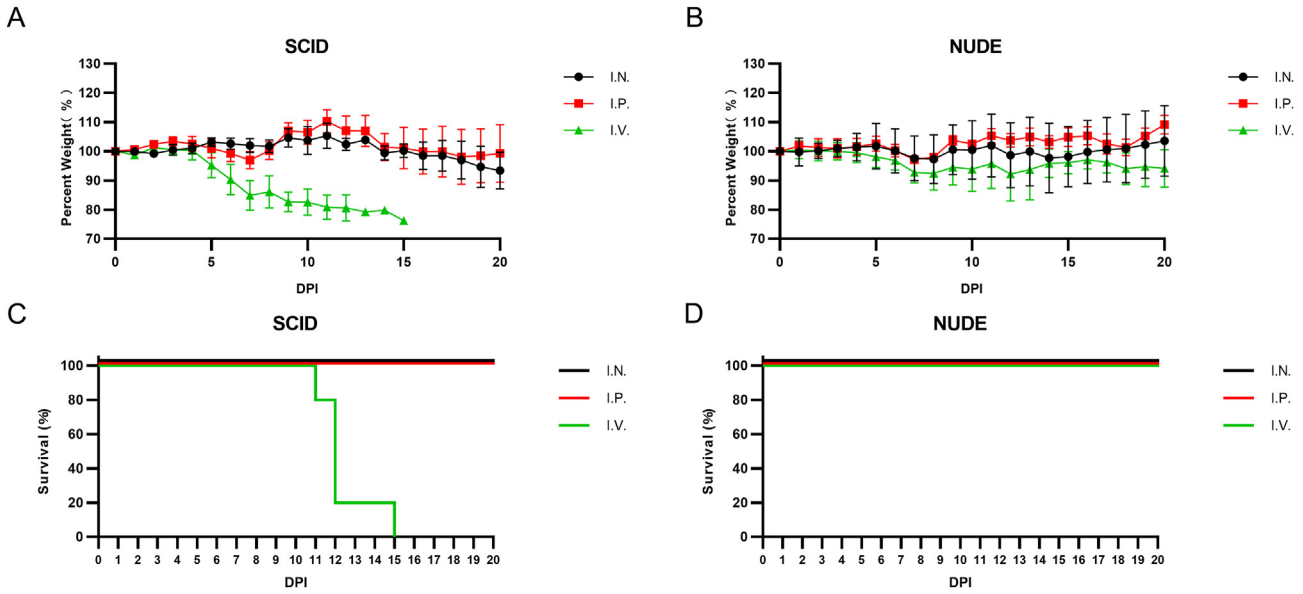

Fig. 5. Body weight changes and mortality rates of severe combined immune-deficiency (SCID) and nude mice following MPXV infection via different routes. SCID and nude mice were divided into three groups, with five mice per group. Each group was infected with $10^{4.5}$ $TCID_{50}$ (100 μL) of MPXV via different inoculation routes. Body weight changes and mortality were daily monitored. **A, B** Body weight changes in SCID mice and nude mice. **C, D** Mortality rates of SCID mice and nude mice. I.N.: intranasal; I.P.: intraperitoneal; I.V.: intravenous. DPI: days post-infection.

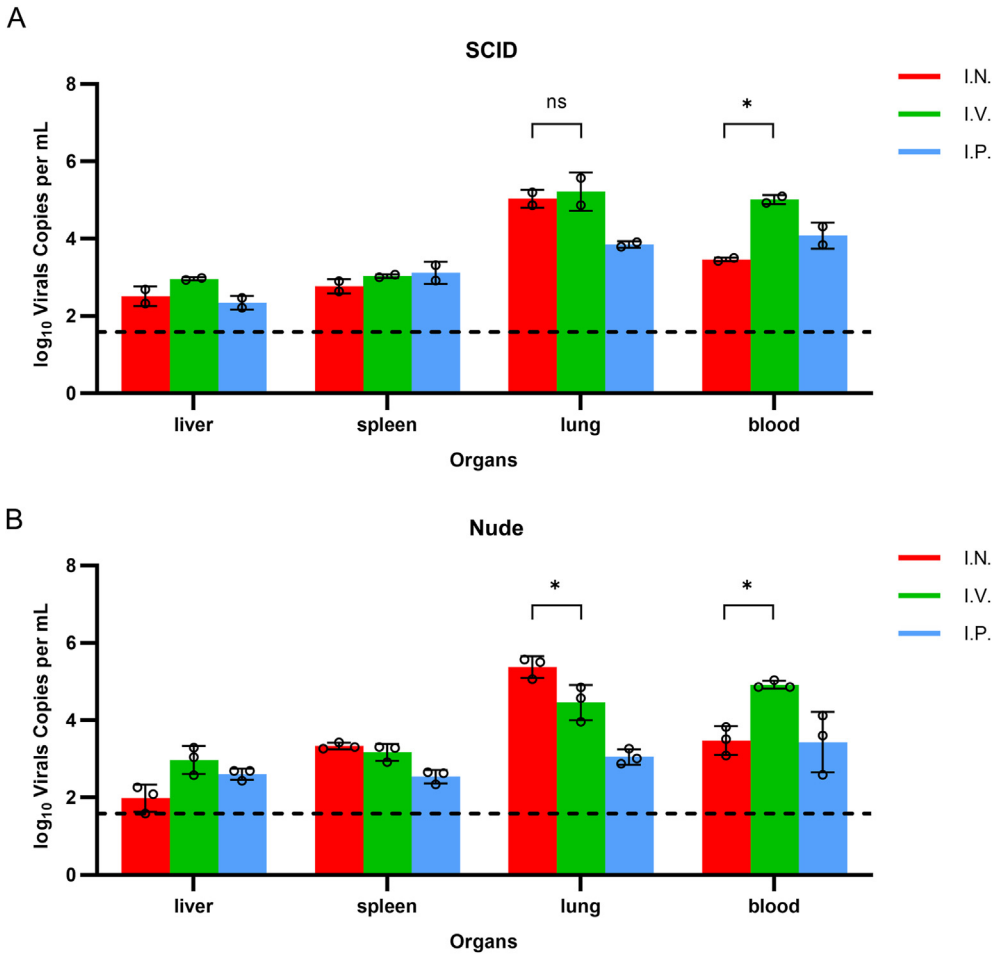

Fig. 6. Tissue viral load of MPXV in severe combined immune-deficiency (SCID) and nude mice following infection via different routes at 9 days post-infection. SCID and nude mice were divided into three groups, with three mice per group. Each group was infected with $10^{4.5}$ $TCID_{50}$ (100 μL) of MPXV via different inoculation routes. The viral loads in tissues at day 9 post-infection were determined by qRT-PCR. **A** MPXV viral load in SCID mouse tissues following different infection routes. **B** MPXV viral load in nude mouse tissues following different infection routes. Data are presented as mean ± SEM. $^*P < 0.05$. I.N.: intranasal; I.P.: intraperitoneal; I.V.: intravenous.

DISCUSSION

Animal models play a crucial role in simulating clinical conditions for disease research. Inbred mouse is the main experimental model for most viruses because of the availability of immunological reagents, inbred strains, easy breeding and commercial availability. Chen et al. investigated the infection characteristics of human adenovirus type 5 (HAdV-5) in inbred BALB/c mice and successfully established a murine model suitable for HAdV vaccine development and anti-adenoviral therapeutic research (Chen et al., 2024). While inbred mouse strains offer certain advantages not found in other animal models, their inherent immunity presents a limitation. Since these strains are not naturally infected with pathogens, most conventional inbred mouse strains exhibit a degree of immune resistance to MPXV, which can influence the interpretation of infection outcomes.

Previous studies have screened 38 inbred mouse strains for susceptibility to MPXV, with the CAST/EiJ strain identified as particularly susceptible (Americo et al., 2010). Statistically significant differences in virulence of clades (I > IIa > IIb) were found in this model. The predominant 2022 outbreak strain did not cause weight loss or lethality in CAST/EiJ mice compared with the lethality of similar doses of clade I and IIa viruses, suggesting that the transmission of clade IIb in humans correlates with diminished virulence for rodents (Americo et al., 2023). Additionally, Osorio et al. conducted research on the *in vivo* imaging of MPXV infection using SCID mice (Osorio et al., 2009). In this study, we investigated the susceptibility of six mouse strains—SCID, nude, db/db, ob/ob, C57BL/6J, and BALB/C—to MPXV infection. SCID and nude mice are immunodeficient models, with SCID mice lacking T and B cell functions, while nude mice have a thymic deficiency. The db/db and ob/ob mice serve as genetic models for obesity and metabolic dysfunction, whereas the C57BL/6J and BALB/C strains are immunocompetent and serve as controls. Our results demonstrate that C57BL/6J and BALB/C mice are resistant to MPXV infection, which is consistent with previous reports indicating that these mouse strains possess innate resistance to MPXV (Earl et al., 2015). However, despite the metabolic dysregulation associated with obesity in db/db and ob/ob mice, these strains did not exhibit increased susceptibility to MPXV infection. In contrast, SCID mice which lack T and B cell functions, and nude mice which have a thymic deficiency, exhibited significant susceptibility to MPXV infection. We hypothesize that the infection process of MPXV may be influenced by the absence of these immune cell populations. Nevertheless, the findings of this study are insufficient to confirm this hypothesis, necessitating further investigation in future research.

Following MPXV infection via the I.N. route in six different mouse strains, we observed a significant weight loss in both SCID and nude mice. While nude mice did not exhibit mortality, SCID mice showed a 100% mortality rate ($n = 5$). No significant weight loss or mortality was observed in the other four strains. These findings are consistent with our observations from MPXV infection via the I.N. route, indicating poor susceptibility to MPXV in the latter four strains. Viral load analysis of different tissues in SCID and nude mice revealed that MPXV replication was predominantly localized to the lung tissue, suggesting the lungs as the primary target organ for MPXV proliferation in immunodeficient mice. Despite similar viral loads in the lungs of SCID mice, mortality rates were significantly different, which we hypothesize could be due to the more severe immune deficiency in SCID mice.

In our investigation of the differences in MPXV susceptibility following various infection routes, we found that SCID and nude mice infected via the I.V. route exhibited more significant weight loss compared to those infected via I.N. and I.P. routes, with SCID mice showing the most pronounced effect. We hypothesize that the enhanced effect of I.V. infection compared to I.N. and I.P. routes may be attributed to the ability of the I.V. route to rapidly deliver the virus throughout the entire body, bypassing local immune barriers, thereby facilitating more efficient viral dissemination and infection. In SCID mice infected via the I.V. route, viral loads in the lung tissue were higher compared to the I.N. group. Conversely, in nude mice, the viral load in the lung tissue of the I.N. group was slightly higher than in the I.V. group. We speculate that this difference may be due to the more severe immune deficiency in SCID mice. This phenomenon underscores the importance of considering the impact of immune deficiency on MPXV susceptibility.

CONCLUSIONS

In conclusion, this study compared the susceptibility of six mouse strains—SCID, nude, db/db, ob/ob, C57BL/6J, and BALB/C—to MPXV infection. We found that immune-deficient mice, including SCID and nude mice, are susceptible to MPXV infection, with the I.V. route proving to be more effective for viral infection in these mice. Our findings highlight the potential of using immune-deficient mouse models, particularly via I.V. inoculation, for more efficient establishment of MPXV infection models. Effective animal infection models not only provide valuable insights into the pathogenic mechanisms of MPXV but also offer critical support for the development of vaccines and therapeutic agents.

MATERIALS AND METHODS

Viruses

The MPXV strain hMpxV/China/GZ8H-01/2023 (GeneBank: PP778666.1, clade IIb) used in this study was isolated from a patient in Guangzhou, China. The virus was propagated in Vero E6 cells and cultured in DMEM (Sigma-Aldrich) supplemented with 10% fetal bovine serum (Invitrogen), 50 U/mL penicillin, and 50 μg/mL streptomycin. All experiments involving infectious MPXV were conducted in an Animal Biosafety Level 3 (ABSL-3) laboratory.

Animal studies

Intranasal infection experiments were conducted using male mice at 8 weeks of age, including SCID (21 ± 1 g) (Beijing, Vital River), nude (24 ± 1 g) (Suzhou, Xishan Bio), db/db (39.5 ± 2 g) (Suzhou, Xishan Bio), ob/ob (39.5 ± 1 g) (Suzhou, Xishan Bio), C57BL/6J (24 ± 1 g) (Suzhou, Xishan Bio), and BALB/C (20 ± 1.5 g) (Suzhou, Xishan Bio) mice. The infection dose was $10^{5.5}$ $TCID_{50}$ in a volume of 100 μL. For weight monitoring, each group consisted of 5 mice, while for sampling, each group consisted of 3 mice.

MPXV infection experiments via three different inoculation routes were conducted using 8-week-old male SCID (Beijing, Vitonglihua) and nude (Suzhou, Xishan Bio) mice. The mice were divided into three groups based on the route of infection: intranasal, intraperitoneal, and intravenous, with each group consisting of 8 mice. These were further divided into two subgroups: the weight monitoring group (5 mice) and the sampling group (3 mice). All mice were inoculated with $10^{4.5}$ $TCID_{50}$ MPXV in a volume of 100 μL via the respective routes.

All animal procedures were performed in ABSL-3 facilities. For all MPXV infection studies, mice were anesthetized in a closed chamber containing isoflurane. Body weight changes and mortality were monitored daily for a total duration of 21 days. All test animals were kept in the same environment as the control animals, with sufficient water and food, and bedding was changed regularly. At the end of the test, all test animals were anesthetized with isoflurane and sacrificed according to animal welfare standards.

Virus detection

In the intranasal MPXV infection experiments with six mouse strains, tissues from all mice in the sampling groups were collected at 6, 12, and 18 days post-infection. Samples included the lungs, liver, spleen, heart, kidneys, brain, rectum, and testes, which were homogenized for analysis. In the MPXV infection experiments involving different inoculation routes in SCID and nude mice, tissues from the liver, spleen, and lungs, as well as

whole blood (without plasma separation), were collected from three mice in the sampling groups at 9 DPI.

All tissues were homogenized using a tissue homogenizer with phosphate-buffered saline (PBS) as the medium, operating at 70 Hz for 10 min. After homogenization, the samples were centrifuged at 8000×*g* for 5 min, and the supernatant was collected. Viral DNA was extracted using the e.z.n.a.® Viral DNA Kit (OMEGA, D3892, USA) according to the manufacturer's protocol. Absolute quantification of viral copies was performed via qRT-PCR using Eastep® qPCR Master Mix (Promega, SL2062, USA) on an ABI 7500 Real-Time PCR System (Applied Biosystems, CA, USA). The qRT-PCR cycling conditions were as follows: 95 °C for 2 min, followed by 40 cycles of 95 °C for 15 s and 60 °C for 1 min. The specific primers used for detecting the MPXV *F3L* gene were as follows:

Forward: 5′-CATCTATTATAGCATCAGCATCAGA-3′

Reverse: 5′-GATACTCCTCCTCGTTGGTCTAC-3′.

Histopathological examination

Lung tissues collected from sampled mice were fixed in 4% paraformaldehyde for histopathological analysis. Fixed tissues were embedded in paraffin, sectioned, and stained with hematoxylin and eosin. Histological changes were then observed under a microscope.

Statistical analysis

Statistical differences between groups were analyzed using GraphPad Prism, Version 8.0. All experimental data are presented as mean ± SD or mean ± SEM. Statistical significance was determined using *t*-tests or ANOVA followed by post-hoc two-tailed *t*-tests. Statistical significance was denoted as $^{*}P < 0.05$.

DATA AVAILABILITY

The authors confirm that the data supporting the findings of this study are available within the article.

ETHICS STATEMENT

All animal studies were conducted in strict accordance with the guidelines of animal welfare of the World Organization for Animal Health (WOAH). All animal experiments were approved by the Institutional Animal Care and Use Committee (IACUC) of the Changchun Veterinary Research Institute, under the protocol number AMMS-11-2023-007. All experiments with MPXV were performed in a biosecurity level 3 laboratory (ABSL-3) approved by Changchun Veterinary Research Institute of the Chinese Academy of Agricultural Sciences.

AUTHOR CONTRIBUTIONS

Xiaohan Wang: conceptualization, data curation, methodology, writing-original draft, writing-review & editing. Shaowen Shi: data curation, investigation, validation. Xiaoxuan Nie: software, validation, writing-review & editing. Yongyang Sun: investigation, software. Jinglei Hu: software, supervision, visualization. Manlin He: project administration, software, visualization. Wenhao Ren: investigation, software. Yuxing Wang: methodology, software. Zhendong Guo: conceptualization, supervision. Gonghe Li: conceptualization, software, supervision. Changbo Ou: formal analysis, resources, supervision. Xiao Li: formal analysis, funding acquisition, validation. Zongzheng Zhao: formal analysis, funding acquisition, methodology, resources, supervision, validation.

CONFLICT OF INTEREST

The authors declare that they have no conflict of interest.

ACKNOWLEDGEMENTS

We acknowledge the Guangzhou Eighth People's Hospital of Guangzhou Medical University for kindly providing the clinical mpox sample, which was utilized to isolate the hMpxV/ChinaGZ8H-01/2023 strain. This work was financially supported by the National Key Research and Development Program of China (No. 2023YFD1800403 and 2023YFD1800404).

REFERENCES

Americo, J.L., Earl, P.L., Moss, B., 2023. Virulence differences of mpox (monkeypox) virus clades I, IIa, and IIb.1 in a small animal model. Proc. Natl. Acad. Sci. U. S. A. 120, e2220415120.

Americo, J.L., Moss, B., Earl, P.L., 2010. Identification of wild-derived inbred mouse strains highly susceptible to monkeypox virus infection for use as small animal models. J. Virol. 84, 8172–8180.

Branche, A., Ramesh, M., Francis, B., 2024. A narrative review of key risk factors for severe illness following SARS-CoV-2, influenza virus, and respiratory syncytial virus infection. Infect. Dis. Ther. 14, 39–61.

Bunge, E.M., Hoet, B., Chen, L., Lienert, F., Weidenthaler, H., Baer, L.R., Steffen, R., 2022. The changing epidemiology of human monkeypox-A potential threat? A systematic review. PLoS Neglected Trop. Dis. 16, e0010141.

Chen, D., Yan, Y., Mei, T., Yang, P., Deng, S., Li, Y., Zhao, T., Xin, N., Duan, B., Liang, W., Yang, Y., Zhao, W., Seto, D., Ou, J., Zhang, Q., 2024. Construction and validation of a mouse model for studying severe human adenovirus infections. Virol. Sin. 39, 963–973.

Coleman, D.L., 1978. Obese and diabetes: two mutant genes causing diabetes-obesity syndromes in mice. Diabetologia 14, 141–148.

Earl, P.L., Americo, J.L., Moss, B., 2015. Genetic studies of the susceptibility of classical and wild-derived inbred mouse strains to monkeypox virus. Virology 481, 161–165.

Everard, A., Lazarevic, V., Derrien, M., Girard, M., Muccioli, G.G., Neyrinck, A.M., Possemiers, S., Van Holle, A., François, P., de Vos, W.M., Delzenne, N.M., Schrenzel, J., Cani, P.D., 2011. Responses of gut microbiota and glucose and lipid metabolism to prebiotics in genetic obese and diet-induced leptin-resistant mice. Diabetes 60, 2775–2786.

Geurts, L., Lazarevic, V., Derrien, M., Everard, A., Van Roye, M., Knauf, C., Valet, P., Girard, M., Muccioli, G.G., François, P., de Vos, W.M., Schrenzel, J., Delzenne, N.M., Cani, P.D., 2011. Altered gut microbiota and endocannabinoid system tone in obese and diabetic leptin-resistant mice: impact on apelin regulation in adipose tissue. Front. Microbiol. 2, 149.

Giesbertz, P., Padberg, I., Rein, D., Ecker, J., Höfle, A.S., Spanier, B., Daniel, H., 2015. Metabolite profiling in plasma and tissues of ob/ob and db/db mice identifies novel markers of obesity and type 2 diabetes. Diabetologia 58, 2133–2143.

Hennessee, I., Shelus, V., McArdle, C.E., Wolf, M., Schatzman, S., Carpenter, A., Minhaj, F.S., Petras, J.K., Cash-Goldwasser, S., Maloney, M., Sosa, L., Jones, S.A., Mangla, A.T., Harold, R.E., Beverley, J., Saunders, K.E., Adams, J.N., Stanek, D.R., Feldpausch, A., Pavlick, J., Cahill, M., O'Dell, V., Kim, M., Alarcón, J., Finn, L.E., Goss, M., Duwell, M., Crum, D.A., Williams, T.W., Hansen, K., Heddy, M., Mallory, K., McDermott, D., Cuadera, M.K.Q., Adler, E., Lee, E.H., Shinall, A., Thomas, C., Ricketts, E.K., Koonce, T., Rynk, D.B., Cogswell, K., McLafferty, M., Perella, D., Stockdale, C., Dell, B., Roskosky, M., White, S.L., Davis, K.R., Milleron, R.S., Mackey, S., Barringer, L.A., Bruce, H., Barrett, D., D'Angeli, M., Kocharian, A., Klos, R., Dawson, P., Ellington, S.R., Mayer, O., Godfred-Cato, S., Labuda, S.M., McCormick, D.W., McCollum, A.M., Rao, A.K., Salzer, J.S., Kimball, A., Gold, J.A.W., 2022. California department of public Health Monkeypox pediatric working group, CDC monkeypox pediatric working group, 2022. Epidemiologic and clinical features of children and adolescents aged <18 Years with Monkeypox - United States, May 17-September 24. MMWR Morb. Mortal. Wkly. Rep. 71, 1407–1411.

Kumar, N., Acharya, A., Gendelman, H.E., Byrareddy, S.N., 2022. The 2022 outbreak and the pathobiology of the monkeypox virus. J. Autoimmun. 131, 102855.

Laurenson-Schafer, H., Sklenovská, N., Hoxha, A., Kerr, S.M., Ndumbi, P., Fitzner, J., Almiron, M., de Sousa, L.A., Briand, S., Cenciarelli, O., Colombe, S., Doherty, M., Fall, I.S., García-Calavaro, C., Haussig, J.M., Kato, M., Mahamud, A.R., Morgan, O.W., Nabeth, P., Naiene, J.D., Navegantes, W.A., Ogundiran, O., Okot, C., Pebody, R., Matsui, T., Ramírez, H.L.-G., Smallwood, C., Tasigchana, R.F.P., Vaughan, A.M., Williams, G.S., , WHO mpox Surveillance and Analytics team, Mala, P.O., Lewis, R.F., Pavlin, B.I., le Polain de Waroux, O., 2023. Description of the first global outbreak of mpox: an analysis of global surveillance data. Lancet Global Health 11, e1012–e1023.

Osorio, J.E., Iams, K.P., Meteyer, C.U., Rocke, T.E., 2009. Comparison of monkeypox viruses pathogenesis in mice by *in vivo* imaging. PLoS One 4, e6592.

Zhu, M., Ji, J., Shi, D., Lu, X., Wang, B., Wu, N., Wu, J., Yao, H., Li, L., 2022. Unusual global outbreak of monkeypox: what should we do? Front. Med. 16, 507–517.